

# V2X-Radar: A Multi-modal Dataset with 4D Radar for Cooperative Perception

Lei Yang<sup>1</sup>, Xinyu Zhang<sup>1\*</sup>, Chen Wang<sup>2</sup>, Jun Li<sup>1</sup>, Jiaqi Ma<sup>3</sup>, Zhiying Song<sup>1</sup>, Tong Zhao<sup>1</sup>, Ziyang Song<sup>4</sup>  
Li Wang<sup>1</sup>, Mo Zhou<sup>1</sup>, Yang Shen<sup>1</sup>, Kai Wu<sup>5</sup>, Chen Lv<sup>6</sup>

<sup>1</sup> School of Vehicle and Mobility, Tsinghua University; <sup>2</sup> China University of Mining and Technology  
<sup>3</sup> UCLA; <sup>4</sup> Beijing Jiaotong University; <sup>5</sup> ByteDance; <sup>6</sup> Nanyang Technological University

yanglei20@mails.tsinghua.edu.cn; xyzhang@tsinghua.edu.cn; lyuchen@ntu.edu.sg



Figure 1. **A data frame sampled from the V2X-Radar dataset.** Each sample includes data from three sensors: (1) dense point clouds (gray points) from roadside and vehicle-side LiDAR; (2) sparse point clouds (green and blue points) with Doppler information from the roadside and vehicle-mounted 4D Radar; (3) RGB images (top row) from the vehicle’s camera and multi-view roadside cameras. All sensors are temporally and spatially synchronized. Each data frame is manually annotated with 3D boxes across five categories.

## Abstract

Modern autonomous vehicle perception systems often struggle with occlusions and limited perception range. Previous studies have demonstrated the effectiveness of cooperative perception in extending the perception range and overcoming occlusions, thereby enhancing the safety of autonomous driving. In recent years, a series of cooperative perception datasets have emerged; however, these datasets primarily focus on cameras and LiDAR, neglecting 4D Radar—a sensor used in single-vehicle autonomous driving to provide robust perception in adverse weather conditions. In this pa-

per, to bridge the gap created by the absence of 4D Radar datasets in cooperative perception, we present V2X-Radar, the first large-scale, real-world multi-modal dataset featuring 4D Radar. V2X-Radar dataset is collected using a connected vehicle platform and an intelligent roadside unit equipped with 4D Radar, LiDAR, and multi-view cameras. The collected data encompasses sunny and rainy weather conditions, spanning daytime, dusk, and nighttime, as well as various typical challenging scenarios. The dataset consists of 20K LiDAR frames, 40K camera images, and 20K 4D Radar data, including 350K annotated boxes across five categories. To support various research domains, we

have established V2X-Radar-C for cooperative perception, V2X-Radar-I for roadside perception, and V2X-Radar-V for single-vehicle perception. Furthermore, we provide comprehensive benchmarks across these three sub-datasets. We will release all datasets<sup>1</sup> and benchmark codebase<sup>2</sup>.

## 1. Introduction

Perception is critical in autonomous driving. While many single-vehicle perception methods [14, 16, 22, 23, 23, 25, 26, 28, 29, 43, 54] have emerged, substantial safety challenges persist due to occlusions and limited perception ranges. These issues occur because vehicles can only view their surroundings from a single perspective, resulting in an incomplete understanding of the scenario. This limitation hinders autonomous vehicles from achieving safe navigation and making optimal decisions. To address this challenge, recent studies have explored cooperative perception, where ego vehicles extend their perception range and overcome occlusions with assistance from other vehicles or roadside perception [31, 41, 42, 44, 45].

Recently, cooperative perception has attracted increasing attention, and several pioneering datasets have been released to bolster this research. For instance, datasets like OpenV2V [37], V2X-Sim [12], and V2XSet [36] are generated through simulations using CARLA [3] and SUMO [10]. In contrast, datasets such as DAIR-V2X [48], V2X-Seq [49], V2V4Real [39], and V2X-Real [32] are derived from real-world scenarios. However, a common limitation of these datasets is their exclusive focus on camera and LiDAR sensors, neglecting the potential of 4D Radar. This sensor is considered advantageous for robust perception due to its exceptional adaptability to adverse weather conditions, as evidenced in single-vehicle autonomous driving datasets such as K-Radar [19] and Dual-Radar [52].

To address the gap in the 4D Radar dataset for cooperative perception and to facilitate related studies, we present V2X-Radar, the first large-scale real-world multi-modal dataset featuring 4D Radar. This dataset includes a diverse range of scenarios, covering various weather conditions such as sunny, rainy, and snowy environments, and spans different times of the day, including daytime, dusk, and nighttime. The data was collected using a connected vehicle platform alongside an intelligent roadside unit, both equipped with 4D Radar, LiDAR, and multi-view cameras (Fig. 1). From over 15 hours of driving logs, we meticulously selected 50 representative scenarios for the final dataset. It comprises 20K LiDAR frames, 40K camera images, and 20K 4D Radar data, featuring 350K annotated bounding boxes across five object categories. To support a

variety of research areas, V2X-Radar is further divided into three specialised sub-datasets: V2X-Radar-C for cooperative perception, V2X-Radar-I for roadside perception, and V2X-Radar-V for single-vehicle perception. Additionally, we provide comprehensive benchmarks of recent perception algorithms across these three sub-datasets. In comparison to existing real-world cooperative datasets, our V2X-Radar demonstrates two key strengths: (1) **More modalities**: The proposed V2X-Radar dataset includes three types of sensors: LiDAR, Camera, and 4D Radar, enabling further exploration into 4D Radar-related cooperative perception research. (2) **Diverse scenarios**: Our data collection covers diverse weather conditions and times of day, focusing on complex intersections that pose challenges for single-vehicle autonomous driving. These scenarios feature obstructed blind spots that impact vehicle safety, providing varied corner cases for cooperative perception research.

Our contributions can be summarized as follows:

- We have developed V2X-Radar, the first extensive real-world multi-modal dataset featuring 4D Radar designed for cooperative perception. All frames are captured through a variety of real-world scenarios using multi-modal sensors.
- We offer 20K LiDAR frames, 40K multi-view camera images, and 20K 4D Radar data, accompanied by 350K annotated bounding boxes across five object categories.
- Comprehensive benchmarks of recent perception algorithms are conducted across cooperative perception on V2X-Radar-C, roadside perception on V2X-Radar-I, and vehicle-side perception on V2X-Radar-V. We will release the entire V2XS-Radar dataset and benchmark codebase.

## 2. Related Works

### 2.1. Autonomous Driving Datasets

Public datasets [1, 12, 19, 27, 32, 36, 37, 39, 48, 49, 52, 53] have significantly accelerated the progress of autonomous driving in recent years. Single-vehicle datasets, such as KITTI [6], NuScenes [1], and Waymo [27], have notably furthered the development of single-vehicle perception. In terms of cooperative perception datasets, OPV2V [37] is the first dataset in this area, gathering data through co-simulation using CARLA [3] and OpenCDA [34, 38]. V2XSet [36] and V2X-Sim [12] explore V2X perception by employing synthesized data from the CARLA simulator [3]. Unlike simulated datasets, DAIR-V2X introduces the first real-world dataset for cooperative detection. V2X-Seq [49] extends sequences from DAIR-V2X [48] with track IDs, establishing a sequential perception and trajectory forecasting dataset. V2V4Real [39] presents the initial real-world V2V dataset gathered from two connected vehicles. V2X-Real [32] is a large-scale multi-modal multi-view dataset intended for V2X research, compiled using

<sup>1</sup><http://openmpd.com/column/V2X-Radar>

<sup>2</sup><https://github.com/yanglei18/V2X-Radar>

Table 1. **Comparisons of our proposed V2X-Radar with existing autonomous driving and V2X datasets.** C: Camera, L: Lidar, R: Radar, V2V: vehicle-to-vehicle, V2I: Vehicle-to-infrastructure.

Dataset	Reference	Location	Sensor	V2X	Real	4D Radar	Adverse Weather	Day&Night	#LiDAR	#Images	#4D Radar	#3D Box
OpenV2V [37]	ICRA'22	Carla	L&C	V2V	✗	✗	✗	✗	11K	44K	0	233K
V2X-Set [36]	ECCV'22	Carla	L&C	V2V&I	✗	✗	✗	✗	11K	44K	0	233K
DAIR-V2X [48]	CVPR'22	China	L&C	V2I	✓	✗	✗	✗	39K	39K	0	464K
V2X-Seq [49]	CVPR'23	China	L&C	V2I	✓	✗	✗	✗	39K	39K	0	464K
V2V4Real [39]	CVPR'23	USA	L&C	V2V	✓	✗	✗	✗	20K	40K	0	240K
RCooper [7]	CVPR'24	China	L&C	I2I	✓	✗	✗	✗	30K	50K	0	310K
TUMTraf-V2X[55]	CVPR'24	DE	L&C	V2I	✓	✗	✗	✓	2K	5K	0	29.38K
<b>V2X-Radar</b>	/	China	L&C&R	V2I	✓	✓	✓	✓	20K	40K	20K	350K

two connected automated vehicles and two intelligent roadside units. TUMTraf-V2X [55] is a multimodal, multi-view V2X cooperative perception dataset designed for 3D object detection and tracking in traffic scenarios. A common limitation among the cooperative perception datasets mentioned above is their narrow focus on camera and LiDAR sensors, overlooking the benefits of 4D Radar. 4D Radar is recognized for its superior adaptability to adverse weather conditions, as demonstrated by single-vehicle autonomous driving datasets such as K-Radar [19] and Dual-Radar [52]. Consequently, It's essential to create a comprehensive multimodal dataset that integrates 4D Radar to enhance cooperative perception research.

## 2.2. Cooperative Perception

Cooperative perception aims to extend the range of perception and overcome occlusions in single-vehicle perception by leveraging shared information among connected agents. It can be classified into three main types based on fusion strategies: (1) Early Fusion, which involves transmitting raw sensor data for the ego vehicle to aggregate and predict objects; (2) Late Fusion, which integrates detection results for a consistent prediction; and (3) Intermediate Fusion, which shares and fuses intermediate high-level features. Recent state-of-the-art methods [2, 4, 5, 8, 18, 30, 30, 35, 36, 50, 51] typically follow intermediate fusion, achieving the best trade-off between accuracy and bandwidth requirements. For instance, V2VNet [30] uses a graph neural network to refine features and perform joint perception and prediction iteratively. F-Cooper [2] introduces a pooling mechanism for identifying salient features. CoBEVT [35] introduced local-global sparse attention for improved cooperative BEV map segmentation. V2X-ViT [36] presented a unified vision transformer for multi-agent and multi-scale perception. HM-ViT [8] introduced a 3D heterogeneous graph transformer for camera and LiDAR fusion. FFNet [50] is a novel flow-based feature fusion framework that addresses temporal asynchrony in cooperative 3D object detection through feature flow prediction. HEAL [18] proposed an extensible collaborative perception framework to integrate new heterogeneous agents with minimal integration cost and performance decline.

## 3. V2X-Radar Dataset

To facilitate cooperative perception research using 4D Radar, we introduce V2X-Radar, the first extensive real-world multi-modal dataset featuring 4D Radar. In this section, we first describe the data acquisition in Sec. 3.1; then, we present the data annotation in Sec. 3.2; and finally, we delve into the diverse data distribution and dataset analysis in Sec. 3.3.

### 3.1. Data Acquisition

**Sensor Setup.** The dataset was collected using a connected vehicle-side platform (Fig. 2(a)) and an intelligent roadside unit (Fig. 2(b)). Both units are equipped with sensors, including 4D Radar, LiDAR, and multi-view cameras. Additionally, a GPS/IMU system is employed to achieve high-precision localisation, facilitating the initial point cloud registration between the vehicle-side and roadside platforms. A C-V2X unit is also integrated for wireless data transmission. The sensor layout configuration can be found in Fig. 2, while detailed specifications are listed in Tab. 2.

**Synchronization.** For cooperative perception datasets, synchronising sensors on both vehicle-side and roadside platforms using a uniform timestamp standard is crucial. To ensure consistency, all computer clocks are initially aligned with GPS time. Hardware-triggered synchronisation of LiDAR, cameras, and 4D Radar is then implemented using the Precision Time Protocol (PTP) and Pulse Per Second (PPS) signals. Subsequently, the closest LiDAR frames from the vehicle-side and roadside platforms are matched, and the camera and 4D Radar data are aligned with each corresponding LiDAR frame to create unified multi-modal data frames. Finally, the time difference between sensors across the two platforms is kept below 20 milliseconds for each sample.

**Sensor Calibration and Registration.** Through the sensor calibration process, we achieve spatial synchronisation of the camera, LiDAR, and 4D Radar. The intrinsic parameters of the camera are calibrated using a checkerboard pattern. In contrast, the LiDAR is calibrated relative to the camera by utilising 100 point pairs extracted from the point cloud and the corresponding camera image. The extrinsic param-

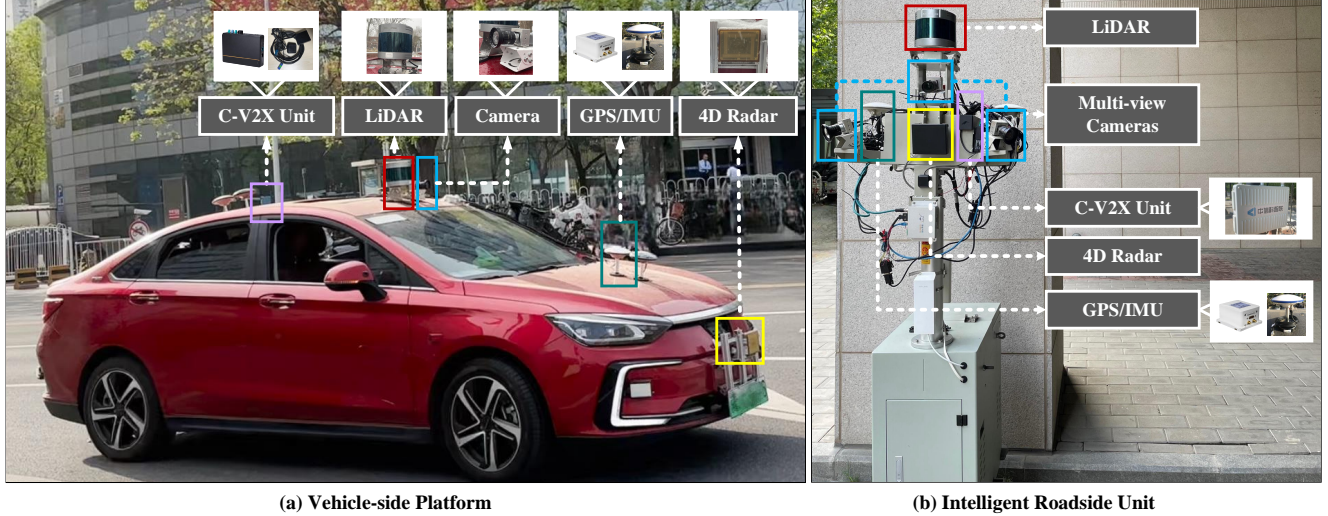


Figure 2. **The sensor configuration on the connected vehicle-side platform and the intelligent roadside unit.** a) the vehicle-side platform, and b) the intelligent roadside unit or infrastructure unit. Both are equipped with multi-modal sensors, including cameras, LiDAR, and 4D Radar, along with a C-V2X unit and a GPS/IMU system.

Table 2. **Sensor specifications in V2X-Radar dataset.** ‘Infra.’ means infrastructure or intelligent roadside unit.

Agent	Sensor	Sensor Model	Details
Infra.	LiDAR	RoboSense RS-Ruby-80 ( $\times 1$ )	80 beams, 360° horizontal FOV, $-25^\circ$ to $+25^\circ$ vertical FOV
	Camera	Basler acA1920-40gc ( $\times 3$ )	RGB, 1536 $\times$ 864 resolution
	4D Radar	OCULI EAGLE ( $\times 1$ )	79.0GHz, $-56^\circ$ to $+56^\circ$ horizontal FOV, $-22^\circ$ to $+22^\circ$ vertical FOV
	C-V2X Unit	VU4004 ( $\times 1$ )	PC5/4G LTE/V2X Protocol
	GPS/IMU	XW-GI5651 ( $\times 1$ )	1000Hz update rate, Double-Precision
Vehicle	LiDAR	RoboSense RS-Ruby-80 ( $\times 1$ )	80 beams, 360° horizontal FOV, $-25^\circ$ to $+25^\circ$ vertical FOV
	Camera	Basler acA1920-40gc ( $\times 1$ )	RGB, 1920 $\times$ 1080 resolution
	4D Radar	Arbe Phoenix ( $\times 1$ )	77GHz, $-50^\circ$ to $+50^\circ$ horizontal FOV, $-15^\circ$ to $+15^\circ$ vertical FOV
	C-V2X Unit	VU4004 ( $\times 1$ )	PC5/4G LTE/V2X Protocol
	GPS/IMU	XW-GI5651 ( $\times 1$ )	1000Hz update rate, Double-Precision

eters are derived by minimising the reprojection errors between the 2D-3D point correspondences. The calibration of the LiDAR with the 4D Radar is conducted by selecting 100 high-intensity point pairs located on corner reflectors. The results of this calibration are visually represented in Fig. 3. Vehicle-side LiDAR alignment with roadside LiDAR is achieved through point cloud registration, initially computed using RTK localisation and subsequently refined via CBM [24] and manual adjustments. The visualisation of the point cloud registration is shown in Fig. 4.

**Data Collection.** We collected 15 hours of driving data, comprising 540K frames and capturing various weather conditions, such as sunny, rainy, foggy, and snowy, across daytime, dusk, and nighttime, as well as typical challenging intersection scenarios. Further details can be found in the supplementary materials. From this, we manually selected the most representative 40 sequences to form V2X-Radar-C; each sequence lasts between 10 to 25 seconds,

with a capturing frequency of 10 Hz. Based on this, we also sampled 10 vehicle-only sequences to create V2X-Radar-V and sampled an additional 10 infrastructure-only sequences to form V2X-Radar-I. In comparison to the single-view data in V2X-Radar-C, both V2X-Radar-V and V2X-Radar-I encompass a wider variety of scenes. Consequently, these three sub-datasets collectively included 20K LiDAR frames, 40K camera images, and 20K 4D Radar data.

### 3.2. Data Annotation.

**Coordinate System.** Our dataset includes four types of coordinate systems: (1) LiDAR coordinate system, where the X, Y, and Z axes align with the front, left, and upward directions of the LiDAR. (2) Camera coordinate systems, in which the z-axis denotes depth. (3) 4D Radar coordinate system, with the X, Y, and Z axes oriented towards the right, front, and upward directions. (4) Global coordinate system, aligning with the LiDAR frame on the roadside platform.

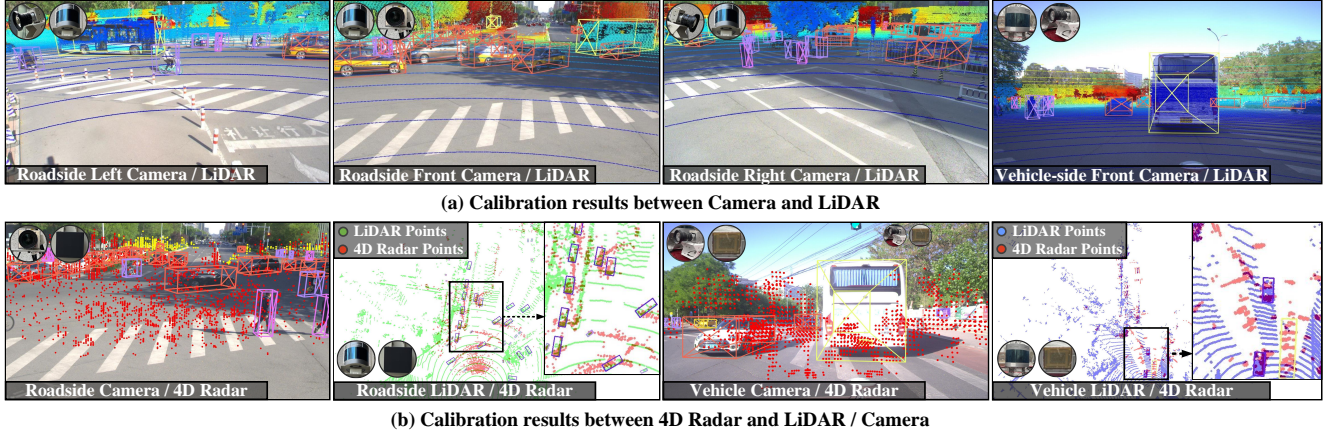


Figure 3. **Visualization of calibration results.** a) The calibration results between the camera and LiDAR. b) The calibration results between the 4D Radar and LiDAR / Camera. The LiDAR points are projected onto the camera plane using the camera’s intrinsic parameters and the camera-LiDAR extrinsics. Similarly, the 4D Radar points are transferred to the LiDAR coordinate system using the 4D Radar-LiDAR extrinsics. Additionally, these 4D Radar points are also mapped onto the camera plane by employing the camera’s intrinsic parameters, along with the extrinsic parameters of the camera-LiDAR and 4D Radar-LiDAR.

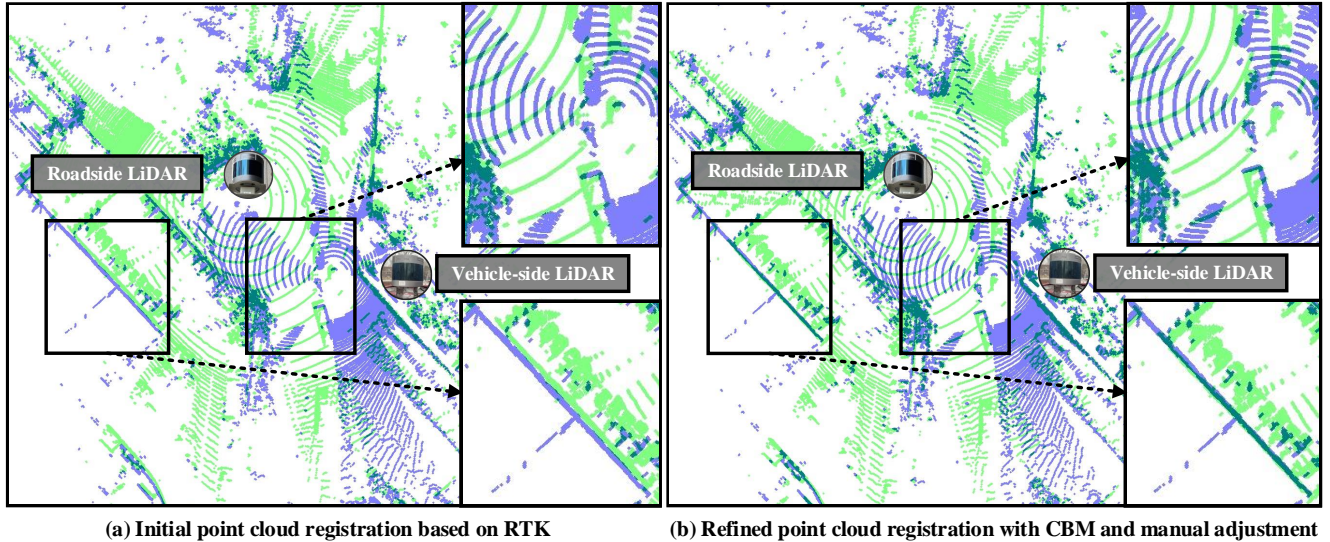


Figure 4. **Visualization of point cloud registration results.** a) Initial point cloud registration based on RTK localization. b) Refined point cloud registration with CBM [24] and manual adjustment. The **blue** points represent the point cloud from the vehicle-side LiDAR, while the **green** points indicate the point cloud from the roadside LiDAR.

**3D Bounding Boxes Annotation.** Data annotation encompasses annotations for vehicles, roadsides, and collaborative efforts. Vehicle and roadside annotations are manually created within their respective LiDAR coordinate systems. For collaborative annotation, we first align the vehicle-side and roadside annotations within a unified roadside LiDAR coordinate system, then match them using the Intersection over Union (IoU) metric to remove duplicates. The annotation process involves five object categories: pedestrian, cyclist, car, bus, and truck. Each object annotation includes attributes such as occlusion and truncation, alongside

the geometric properties of 3D bounding boxes, denoted as  $(x, y, z, w, h, l, \theta)$ , where  $(l, w, h)$  represent the object’s dimensions,  $(x, y, z)$  indicate its location, and  $heta$  denotes its orientation.

### 3.3. Data Analysis

Fig. 5(a) illustrates the distribution of objects across five categories under both day and night conditions, with cars being the most prevalent in V2X-Radar, followed by cyclists and pedestrians, while trucks and buses are the least common. Fig. 5(b) displays the maximum and average

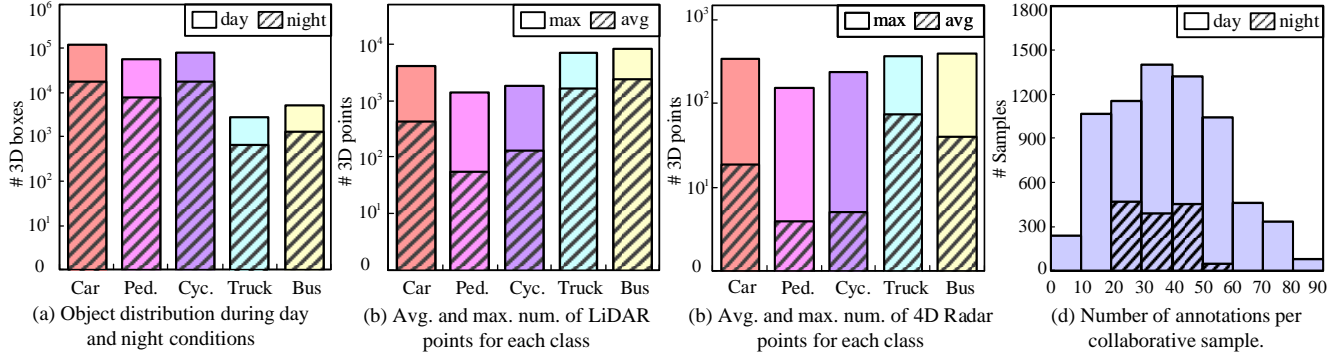


Figure 5. **Data analysis of our V2X-Radar dataset.** a) Distribution of objects during day and night conditions. b) Average and maximum number of LiDAR points within the 3D bounding box for each category. c) Average and maximum number of 4D Radar points within the 3D bounding box for each category. d) Number of annotations per collaborative sample. The vertical axes of sub-plots (a)-(c) use a log scale, whilst the vertical axis of sub-plot (d) employs a standard scale.

number of LiDAR points within 3D bounding boxes for each category, suggesting that larger vehicles possess more 3D points than smaller pedestrians or cyclists. Fig. 5(c) reveals the density distribution of 4D Radar points within various objects’ bounding boxes, reflecting a trend similar to that shown in Fig. 5(b). Lastly, Fig. 5(d) indicates that annotations per collaborative sample can reach up to 90 - a significant increase compared to single-vehicle datasets such as KITTI [6] or nuScenes [1], emphasising how the integration of vehicle-side and roadside data enhances the comprehensiveness of environmental perception.

## 4. Tasks

V2X-Radar dataset comprises three sub-datasets: V2X-Radar-I, V2X-Radar-V, and V2X-Radar-C, which are designed for roadside 3D object detection, single-vehicle 3D object detection, and cooperative 3D object detection.

### 4.1. Single-agent 3D Object Detection

**Task Definition.** Single-agent 3D object detection involves two distinct tasks: roadside 3D object detection using the V2X-Radar-I sub-dataset, and vehicle-side 3D object detection employing the V2X-Radar-V sub-dataset. These tasks utilise sensors from either the intelligent roadside unit or the vehicle-side platform for 3D object detection, presenting the following challenges:

- **Single-modal Encoding:** The process of encoding a 2D image from the camera, a dense 3D point cloud from LiDAR, and a sparse point cloud with Doppler information from 4D Radar into a 3D spatial representation is essential for precise single-modal 3D object detection.
- **Multi-modal Fusion:** When fusing multi-modal information from various sensors, it is essential to account for (1) spatial misalignment, (2) temporal misalignment, and (3) sensor failure. Addressing these issues is crucial for achieving robust multi-modal 3D object detection.

**Evaluation Metrics.** The evaluation area covers  $[-100, 100]$  in x direction and  $[0, 100]$  in y direction from the ego-vehicle or roadside unit. Following the metrics in Rope3D [46], KITTI [6] datasets, we utilize the Average Precision (AP) at IoU thresholds of 0.5 and 0.7 to evaluate the performance of object detection.

**Benchmark Methods.** We conduct a comprehensive evaluation of various leading single-agent 3D object detectors based on different sensor inputs. Specifically, our evaluation encompasses LiDAR-centric techniques such as PointPillars [11], SECOND [40], CenterPoint [47], and PV-RCNN [21]; camera-dependent methods including SMOKE [15], BVDepth [13], BEVHeight [42], and BEVHeight++ [41]; and 4D Radar-based approaches like RPFA-Net [33] and RDIOU [20].

### 4.2. Cooperative 3D Object Detection

**Task Definition.** The cooperative 3D object detection task with the V2X-Radar-C sub-dataset aims to utilise sensors from both the vehicle-side platform and the intelligent roadside unit to execute 3D object detection for the ego-vehicle. In contrast to the previous single-agent perception, cooperative perception presents domain-specific challenges:

- **Spatial Asynchrony:** Localization errors can create discrepancies in the relative pose between the single-vehicle and the intelligent roadside unit, potentially leading to global misalignment when translating data from the roadside unit to the ego-vehicle coordinate systems.
- **Temporal Asynchrony:** Communication delays in the data transmission process can result in timestamp discrepancies between the sensor data from the single-vehicle platform and the intelligent roadside unit. This may cause local misalignment of dynamic objects when translating data within the same coordinate systems.

**Evaluation Metrics.** The evaluation area spans  $[-100, 100]$  metres in both the x and y directions relative to the ego ve-

Table 3. **Roadside 3D object detection benchmarks on V2X-Radar-I under homogeneous split.** The vehicle category includes car, bus and truck. ‘M’ means modality, and L, C, and R denote LiDAR, Camera, and 4D Radar, respectively.

Method	M	Vehicle (IoU = 0.7 / 0.5)			Pedestrian (IoU = 0.5 / 0.25)			Cyclist (IoU = 0.5 / 0.25)		
		Easy	Moderate	Hard	Easy	Moderate	Hard	Easy	Moderate	Hard
Pointpillars [11]	L	78.00 / 88.69	71.24 / 81.16	71.24 / 81.16	53.87 / 69.61	52.94 / 67.09	52.94 / 67.09	80.01 / 87.48	72.67 / 78.60	72.67 / 78.60
SECOND [40]	L	81.61 / 91.06	74.34 / 83.47	74.34 / 83.47	57.56 / 74.64	55.39 / 72.27	55.39 / 72.27	80.53 / 87.68	74.06 / 80.62	74.06 / 80.62
CenterPoint [47]	L	86.44 / 94.04	78.98 / 84.26	78.98 / 84.26	67.90 / 84.74	65.39 / 81.35	65.39 / 81.35	90.26 / 92.91	82.87 / 85.51	82.87 / 85.51
PV-RCNN [21]	L	88.83 / 94.11	81.39 / 86.61	81.39 / 86.61	77.13 / 86.39	74.66 / 83.87	74.66 / 83.87	91.82 / 94.44	84.47 / 87.08	84.46 / 87.08
SMOKE [15]	C	22.05 / 58.43	20.72 / 56.36	20.69 / 56.31	8.26 / 25.64	7.68 / 24.36	7.63 / 24.30	12.50 / 38.29	11.28 / 36.40	11.24 / 36.36
BEVDepth [13]	C	45.01 / 69.25	42.23 / 66.81	42.21 / 66.75	30.64 / 61.46	29.13 / 59.11	29.10 / 59.05	39.85 / 68.71	38.52 / 67.05	38.43 / 67.02
BEVHeight [42]	C	47.91 / 72.45	45.53 / 69.48	45.49 / 67.44	32.08 / 64.06	29.78 / 59.79	29.68 / 59.74	42.97 / 71.63	41.34 / 69.11	41.30 / 69.07
BEVHeight++[41]	C	48.48 / 73.81	47.92 / 70.36	47.88 / 70.32	33.05 / 66.12	32.30 / 64.67	32.32 / 64.66	45.19 / 74.52	44.20 / 72.04	44.14 / 72.01
RDIOU [20]	R	61.38 / 80.03	54.89 / 72.72	54.89 / 72.72	43.82 / 72.03	42.11 / 69.65	42.11 / 69.65	40.74 / 67.31	36.68 / 60.83	36.68 / 60.83
RPFA-Net [33]	R	64.79 / 82.58	58.01 / 75.36	58.01 / 75.36	51.64 / 78.05	49.51 / 73.91	49.51 / 73.91	45.86 / 71.81	41.66 / 64.95	41.66 / 64.95

Table 4. **Single-vehicle 3D object detection benchmarks on V2X-Radar-V under homogeneous split.** The vehicle category includes car, bus and truck. ‘M’ means modality, and L, C, and R denote LiDAR, Camera, and 4D Radar, respectively.

Method	M	Vehicle (IoU = 0.7 / 0.5)			Pedestrian (IoU = 0.5 / 0.25)			Cyclist (IoU = 0.5 / 0.25)		
		Easy	Moderate	Hard	Easy	Moderate	Hard	Easy	Moderate	Hard
Pointpillars [11]	L	75.66 / 83.52	68.80 / 77.07	68.80 / 77.07	41.89 / 46.34	38.16 / 43.18	38.16 / 43.18	78.63 / 83.14	65.24 / 69.77	65.24 / 69.77
SECOND [40]	L	78.35 / 84.34	71.31 / 79.75	71.31 / 79.75	43.74 / 49.75	39.07 / 45.91	39.07 / 45.91	82.88 / 85.12	68.27 / 73.22	68.27 / 73.22
CenterPoint [47]	L	80.87 / 87.74	72.19 / 81.42	72.19 / 81.42	55.27 / 62.63	50.59 / 58.81	50.59 / 58.81	88.21 / 92.48	75.26 / 79.44	75.26 / 79.44
PV-RCNN [21]	L	88.27 / 89.12	79.38 / 84.31	79.38 / 84.31	67.04 / 69.81	58.83 / 65.78	58.83 / 65.78	89.48 / 93.49	78.01 / 81.07	78.01 / 81.07
SMOKE [15]	C	9.86 / 31.92	8.61 / 26.41	8.28 / 24.36	0.23 / 2.02	0.29 / 1.89	0.29 / 1.89	0.39 / 7.23	0.37 / 4.96	0.37 / 4.13
BEVDepth [13]	C	16.91 / 41.63	15.47 / 39.68	15.02 / 37.83	9.92 / 29.98	8.51 / 27.76	8.49 / 27.72	12.18 / 47.20	9.46 / 39.34	9.30 / 39.15
BEVHeight [42]	C	16.58 / 40.32	15.32 / 39.15	14.08 / 37.30	9.49 / 28.50	8.48 / 26.46	8.39 / 26.57	9.58 / 44.56	7.35 / 35.04	7.26 / 34.91
BEVHeight++ [41]	C	17.47 / 43.68	15.53 / 42.24	14.77 / 41.58	10.43 / 31.15	9.36 / 28.85	9.32 / 28.73	12.99 / 49.08	9.91 / 41.10	9.83 / 40.94
RDIOU [20]	R	41.11 / 72.67	29.03 / 54.27	28.37 / 52.02	10.72 / 28.59	9.97 / 26.88	9.84 / 26.78	14.74 / 44.57	10.81 / 31.15	10.67 / 30.91
RPFA-Net [33]	R	42.77 / 75.79	30.44 / 57.27	29.34 / 55.06	11.51 / 30.54	10.37 / 28.15	10.29 / 27.43	17.03 / 46.31	11.98 / 33.96	11.91 / 33.77

hicle. Similar to DAIR-V2X [48] and V2V4Real [39], we group various vehicle types into the same class and concentrate solely on vehicle detection. The performance of object detection is evaluated using Average Precision (AP) at IoU thresholds of 0.5 and 0.7. Transmission costs are calculated through Average MegaBytes (AM). In line with previous studies [39, 48], we compare methods in two configurations: (1) Synchronous, ignoring communication delays. (2) Asynchronous, simulating data transmission delay by retrieving roadside samples with the preceding timestamp.

**Benchmark Methods.** We provide comprehensive benchmarks for the following three fusion strategies in cooperative 3D object detection:

- **Late Fusion:** Each agent employs its sensors to detect 3D objects and shares the predictions. The receiving agent then applies NMS to generate the final outputs.
- **Early Fusion:** The ego vehicle collects all point clouds from itself and other agents into its own coordinate system, then proceeds with detection procedures.
- **Intermediate Fusion:** Each agent employs a neural feature extractor to obtain intermediate features; the encoded features are compressed and transmitted to the ego vehicle for cooperative feature fusion.

We evaluate several prominent intermediate methods, including F-Cooper [2], V2XVIT [36], CoAlign [35], and HEAL [18], to establish a benchmark in this field.

## 5. Experiments

### 5.1. Implementation details

For the dataset split, single-agent 3D object detection, which includes roadside and vehicle-side scenarios, follows two distinct setups: (1) homogeneous split, where the dataset is divided into train/val/test sets containing 7000, 1500, and 1500 frames, respectively. The selection of samples in this setup is entirely random. (2) heterogeneous split, where the dataset is divided into train/val/test sets with 34, 8, and 8 sequences. The cooperative 3D object detection dataset is divided into train/val/test sets with 30, 5, and 5 sequences. Notably, all experimental results are assessed using the validation set. For the detection areas, the single-agent detection techniques cover a range of [0, 100] m in the x-direction and [-100, 100] m in the y-direction relative to the ego vehicle or roadside unit. In contrast, cooperative

Table 5. **Cooperative 3D object detection benchmarks for vehicle category on V2X-Radar-C.** The vehicle category includes car, bus and truck. Sync. means synchronous setup ignoring communication delays. Async. implies asynchronous setup with a 100 ms delay.

Method	M	Sync. (AP@IoU = 0.5 / 0.7)				Async. (AP@IoU = 0.5 / 0.7)				AM (MB)
		Overall	0-30m	30-50m	50-100m	Overall	0-30m	30-50m	50-100m	
No Fusion	L	21.44 / 17.40	22.73 / 18.54	22.22 / 18.60	18.15 / 13.64	21.44 / 17.40	22.73 / 18.54	22.22 / 18.60	18.15 / 13.64	0
Late Fusion	L	54.38 / 35.03	67.09 / 52.93	49.56 / 35.46	32.58 / 20.51	47.84 / 22.11	59.97 / 33.13	42.05 / 20.84	28.27 / 14.78	0.003
Early Fusion	L	58.89 / 49.04	74.13 / 63.74	52.73 / 43.64	34.38 / 28.71	51.09 / 27.22	64.38 / 35.67	43.26 / 22.05	29.93 / 19.08	1.25
F-Cooper [2]	L	60.27 / 45.33	74.91 / 61.87	56.64 / 38.95	35.85 / 21.32	55.56 / 32.03	70.11 / 44.81	50.01 / 23.64	32.48 / 17.31	0.25
CoAlign [17]	L	66.42 / 55.56	70.81 / 63.27	66.75 / 54.15	58.36 / 43.01	58.43 / 35.07	63.32 / 39.61	56.64 / 31.83	50.65 / 31.00	0.25
HEAL [18]	L	67.75 / 57.78	72.78 / 65.59	69.24 / 56.23	57.79 / 45.32	60.75 / 39.27	65.72 / 43.95	59.99 / 36.04	51.41 / 34.52	0.25
No Fusion	C	3.45 / 2.61	5.08 / 1.56	0.69 / 0.29	0.22 / 0.10	3.45 / 2.61	5.08 / 1.56	0.69 / 0.29	0.22 / 0.10	0
Late Fusion	C	12.82 / 7.56	27.33 / 16.53	2.38 / 1.93	1.87 / 0.92	11.08 / 4.68	23.88 / 10.19	1.94 / 1.14	1.59 / 0.58	0.003
V2X-ViT [36]	C	17.51 / 10.54	32.28 / 19.93	3.42 / 2.64	2.34 / 1.39	15.61 / 7.24	29.19 / 13.58	2.95 / 1.71	2.05 / 0.92	0.25
CoAlign [17]	C	19.33 / 12.67	37.01 / 21.05	3.89 / 2.73	2.45 / 1.41	17.33 / 8.61	33.41 / 14.11	3.27 / 1.74	2.17 / 0.97	0.25
HEAL [18]	C	19.58 / 13.56	34.74 / 24.84	4.02 / 2.88	2.80 / 1.53	17.42 / 9.53	31.23 / 17.43	3.43 / 1.96	2.47 / 0.98	0.25
No Fusion	R	6.98 / 3.06	11.63 / 6.62	1.08 / 0.52	0.87 / 0.26	6.98 / 3.06	11.63 / 6.62	1.08 / 0.52	0.87 / 0.26	0
Late Fusion	R	10.95 / 6.87	20.59 / 11.69	1.93 / 1.15	1.21 / 0.54	9.76 / 4.67	18.39 / 7.83	1.44 / 0.74	1.06 / 0.41	0.003
Early Fusion	R	13.65 / 7.37	24.07 / 13.89	2.19 / 1.49	1.25 / 0.71	12.09 / 5.24	21.51 / 9.76	1.67 / 1.01	1.09 / 0.46	0.32
V2X-ViT [36]	R	14.23 / 8.74	25.23 / 14.92	2.84 / 1.77	1.66 / 0.93	12.68 / 6.01	22.82 / 10.17	2.25 / 1.15	1.46 / 0.61	0.25
CoAlign [17]	R	15.59 / 9.76	26.76 / 17.32	3.08 / 1.86	2.05 / 1.23	13.71 / 6.52	23.63 / 11.49	2.41 / 1.16	1.77 / 0.82	0.25
HEAL [18]	R	15.82 / 10.08	27.02 / 18.24	3.56 / 1.91	1.83 / 1.12	13.97 / 7.56	24.11 / 12.97	2.85 / 1.23	1.62 / 0.75	0.25

3D object detection encompasses a broader area, extending from [-100, 100] m in both the x and y directions relative to the ego vehicle. For the ground truth, LiDAR or camera methods utilize all the annotations. Considering the limited coverage area of 4D Radar, 4D Radar-based methods only use labels within its field of view for training and evaluation. For the feature extractor, all cooperative detection methods depend on PointPillar [11] to extract BEV features from LiDAR or 4D Radar point clouds and use LSS [9] to extract BEV features from camera images.

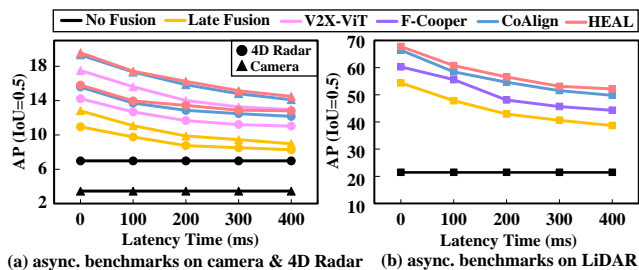


Figure 6. **Cooperative 3D object detection benchmarks on V2X-Radar-C under different transmission delay.**

## 5.2. Benchmark results

**Single-agent 3D Object Detection.** The benchmark results for the V2X-Radar-I and V2X-Radar-V sub-datasets under a homogeneous split are detailed in Tab. 3 and Tab. 4. Further results under the heterogeneous split can be found in the supplementary materials. The experimental results in these tables clearly demonstrate that LiDAR-based methods achieve the highest performance. Although 4D radar-based methods manage a relatively sparse point cloud, they still

outperform camera-based methods. Camera-based methods, restricted by their inability to utilize depth information, are less effective than LiDAR and 4D Radar-based methods. **Cooperative 3D Object Detection.** Tab. 5 presents a quantitative comparison of several methods on V2X-Radar-C:

- In comparison to the benchmark of single-vehicle perception, all methods involving cooperative perception exhibit a significant performance enhancement, highlighting its essential role in improving single-vehicle perception. Compared to the results from the Sync setting, the introduction of communication delay in Async settings led to a considerable performance decline. As shown in Tab. 5 and Fig. 6, when subjected to a 100ms transmission delay with a strict 0.7 IoU threshold, F-Cooper [2], CoAlign [17], and HEAL [18] using LiDAR point cloud experienced significant reductions of 13.30%, 20.49%, and 18.51% respectively. These findings underline the necessity of mitigating the effects of communication delay to ensure effective and robust cooperative perception.

## 6. Conclusion

In this paper, we introduce V2X-Radar, the first large-scale real-world multi-modal dataset featuring 4D Radar for cooperative perception, aiming to prompt cooperative perception with 4D Radar for a broader operational design domain (ODD). Our dataset focuses on challenging intersection scenarios and provides data collected under various times and weather conditions. It consists of 20K LiDAR frames, 40K camera images, and 20K 4D Radar data points, along with 350K annotated bounding boxes 5 categories. To support a wide range of perception research, we organise the dataset

into three sub-datasets: V2X-Radar-C for cooperative perception, V2X-Radar-I for roadside perception, and V2X-Radar-V for single-vehicle perception. Furthermore, we have conducted extensive benchmarks of recent perception algorithms on these three sub-datasets.

**Limitation and Future Work.** Our dataset focuses on 3D object detection, and we simulate asynchronous cooperative perception with a fixed time delay. In the future, we plan to expand our V2X-Radar tasks to include tracking and trajectory prediction, and evaluate performance under real C-V2X communication delays.

## References

- [1] Holger Caesar, Varun Bankiti, Lang Alex H., Vora Sourabh, Liong Venice Erin, Xu Qiang, Krishnan Anush, Yu Pan, Giancarlo Baldan, and Beijbom Oscar. nuscenes: A multi-modal dataset for autonomous driving. In *Proceedings of the IEEE/CVF Conference on Computer Vision and Pattern Recognition*, pages 11618–11628, 2020. 2, 6
- [2] Qi Chen, Xu Ma, Sihai Tang, Jingda Guo, Qing Yang, and Song Fu. F-cooper: Feature based cooperative perception for autonomous vehicle edge computing system using 3d point clouds. In *Proceedings of the 4th ACM/IEEE Symposium on Edge Computing*, pages 88–100, 2019. 3, 7, 8
- [3] Alexey Dosovitskiy, German Ros, Felipe Codevilla, Antonio Lopez, and Vladlen Koltun. Carla: An open urban driving simulator. In *Proceedings of the 1st Annual Conference on Robot Learning*, pages 1–16. PMLR, 2017. 2
- [4] Siqi Fan, Haibao Yu, Wenxian Yang, Jirui Yuan, and Zaiqing Nie. Quest: Query stream for practical cooperative perception. In *2024 IEEE International Conference on Robotics and Automation (ICRA)*, pages 18436–18442, 2024. 3
- [5] Xin Gao, Xinyu Zhang, Yiguo Lu, Yuning Huang, Lei Yang, Yijin Xiong, and Peng Liu. A survey of collaborative perception in intelligent vehicles at intersections. *IEEE Transactions on Intelligent Vehicles*, 2024. 3
- [6] Andreas Geiger, Lenz Philip, and Raquel Urtasun. Are we ready for autonomous driving? the kitti vision benchmark suite. In *Proceedings of the IEEE/CVF Conference on Computer Vision and Pattern Recognition*, pages 3354–3361, 2012. 2, 6
- [7] Ruiyang Hao, Siqi Fan, Yingru Dai, Zhenlin Zhang, Chenxi Li, Yuntian Wang, Haibao Yu, Wenxian Yang, Jirui Yuan, and Zaiqing Nie. Rcooper: A real-world large-scale dataset for roadside cooperative perception. In *Proceedings of the IEEE/CVF Conference on Computer Vision and Pattern Recognition*, pages 22347–22357, 2024. 3
- [8] Xiang Hao, Runsheng Xu, and Ma Jiaqi. Hm-vit: Hetero-modal vehicle-to-vehicle cooperative perception with vision transformer. In *2023 IEEE/CVF International Conference ON Computer Vision (ICCV)*, pages 284–295, 2023. 3
- [9] Junjie Huang, Guan Huang, Zheng Zhu, Yun Ye, and Dalong Du. Bevdet: High-performance multi-camera 3d object detection in bird-eye-view. *arXiv preprint arXiv:2112.11790*, 2021. 8
- [10] Daniel Krajzewicz, Jakob Erdmann, Michael Behrisch, and Laura Bieker. Recent development and applications of sumo - simulation of urban mobility. pages 128–138, 2012. 2
- [11] Alex H Lang, Sourabh Vora, Holger Caesar, Lubing Zhou, Jiong Yang, and Oscar Beijbom. Pointpillars: Fast encoders for object detection from point clouds. In *Proceedings of the IEEE/CVF Conference on Computer Vision and Pattern Recognition*, pages 12697–12705, 2019. 6, 7, 8, 13
- [12] Yiming Li, Dekun Ma, Ziyang An, Zixun Wang, Yiqi Zhong, Siheng Chen, and Chen Feng. V2x-sim: Multi-agent collaborative perception dataset and benchmark for autonomous driving. *IEEE Robotics and Automation Letters*, 7(4):10914–10921, 2022. 2
- [13] Yin hao Li, Zheng Ge, Guanyi Yu, Jinrong Yang, Zengran Wang, Yukang Shi, Jianjian Sun, and Zeming Li. Bevdepth: Acquisition of reliable depth for multi-view 3d object detection. In *Proceedings of the AAAI Conference on Artificial Intelligence*, pages 1477–1485, 2023. 6, 7, 13
- [14] Lin Liu, Ziyang Song, Qiming Xia, Feiyang Jia, Caiyan Jia, Lei Yang, Yan Gong, and Hongyu Pan. Sparsedet: a simple and effective framework for fully sparse lidar-based 3d object detection. *IEEE Transactions on Geoscience and Remote Sensing*, 2024. 2
- [15] Zechen Liu, Zizhang Wu, and Roland Tóth. Smoke: Single-stage monocular 3d object detection via keypoint estimation. In *Proceedings of the IEEE/CVF Conference on Computer Vision and Pattern Recognition Workshops*, pages 996–997, 2020. 6, 7, 13
- [16] Zhijian Liu, Haotian Tang, Alexander Amini, Xinyu Yang, Huizi Mao, Daniela L Rus, and Song Han. Bevfusion: Multi-task multi-sensor fusion with unified bird’s-eye view representation. In *2023 IEEE international conference on robotics and automation (ICRA)*, pages 2774–2781, 2023. 2
- [17] Yifan Lu, Quanhao Li, Baoan Liu, Mehrdad Dianati, Chen Feng, Siheng Chen, and Yanfeng Wang. Robust collaborative 3d object detection in presence of pose errors. In *2023 IEEE International Conference on Robotics and Automation (ICRA)*, pages 4812–4818, 2023. 8
- [18] Yifan Lu, Yue Hu, Yiqi Zhong, Dequan Wang, Siheng Chen, and Yanfeng Wang. An extensible framework for open heterogeneous collaborative perception. In *The Twelfth International Conference on Learning Representations*, 2024. 3, 7, 8
- [19] Dong-Hee Paek, SEUNG-HYUN KONG, and Kevin Tirta Wijaya. K-radar: 4d radar object detection for autonomous driving in various weather conditions. In *Advances in Neural Information Processing Systems*, pages 3819–3829. Curran Associates, Inc., 2022. 2, 3
- [20] Hualian Sheng, Sijia Cai, Na Zhao, Bing Deng, Jianqiang Huang, Xian-Sheng Hua, Min-Jian Zhao, and Gim Hee Lee. Rethinking iou-based optimization for single-stage 3d object detection. In *European Conference on Computer Vision*, pages 544–561. Springer, 2022. 6, 7, 13
- [21] Shaoshuai Shi, Chaoxu Guo, Li Jiang, Zhe Wang, Jianping Shi, Xiaogang Wang, and Hongsheng Li. Pv-rcnn: Point-voxel feature set abstraction for 3d object detection. In *Proceedings of the IEEE/CVF Conference on Computer Vision and Pattern Recognition*, pages 10529–10538, 2020. 6, 7, 13

- [22] Ziyang Song, Caiyan Jia, Lei Yang, Haiyue Wei, and Lin Liu. Graphalign++: An accurate feature alignment by graph matching for multi-modal 3d object detection. *IEEE Transactions on Circuits and Systems for Video Technology*, 2023. 2
- [23] Ziyang Song, Lin Liu, Feiyang Jia, Yadan Luo, Caiyan Jia, Guoxin Zhang, Lei Yang, and Li Wang. Robustness-aware 3d object detection in autonomous driving: A review and outlook. *IEEE Transactions on Intelligent Transportation Systems*, 2024. 2
- [24] Zhiying Song, Tenghui Xie, Hailiang Zhang, Jiabin Liu, Fuxi Wen, and Jun Li. A spatial calibration method for robust cooperative perception. *IEEE Robotics and Automation Letters*, 2024. 4, 5
- [25] Ziyang Song, Guoxing Zhang, Lin Liu, Lei Yang, Shaoqing Xu, Caiyan Jia, Feiyang Jia, and Li Wang. Robofusion: Towards robust multi-modal 3d object detection via sam. In *Proceedings of the Thirty-Third International Joint Conference on Artificial Intelligence, IJCAI-24*, pages 1272–1280. International Joint Conferences on Artificial Intelligence Organization, 2024. Main Track. 2
- [26] Ziyang Song, Lei Yang, Shaoqing Xu, Lin Liu, Dongyang Xu, Caiyan Jia, Feiyang Jia, and Li Wang. Graphbev: Towards robust bev feature alignment for multi-modal 3d object detection. In *European Conference on Computer Vision*, pages 347–366. Springer, 2025. 2
- [27] Pei Sun, Henrik Kretzschmar, Xerxes Dotiwalla, Aurélien Chouard, and Vijaysai Patnaik. Scalability in perception for autonomous driving: Waymo open dataset. In *Proceedings of the IEEE/CVF Conference on Computer Vision and Pattern Recognition*, pages 2443–2451, 2020. 2
- [28] Li Wang, Xinyu Zhang, Wenyuan Qin, Xiaoyu Li, Jinghan Gao, Lei Yang, Zhiwei Li, Jun Li, Lei Zhu, Hong Wang, et al. Camo-mot: Combined appearance-motion optimization for 3d multi-object tracking with camera-lidar fusion. *IEEE Transactions on Intelligent Transportation Systems*, 24(11):11981–11996, 2023. 2
- [29] Li Wang, Xinyu Zhang, Ziyang Song, Jiangfeng Bi, Guoxin Zhang, Haiyue Wei, Liyao Tang, Lei Yang, Jun Li, Caiyan Jia, et al. Multi-modal 3d object detection in autonomous driving: A survey and taxonomy. *IEEE Transactions on Intelligent Vehicles*, 8(7):3781–3798, 2023. 2
- [30] Tsun Hsuan Wang, Manivasagam Sivabalan, Ming Liang, Yang Bin, Wenyuan Zeng, and Raquel Urtasun. V2vnet: Vehicle-to-vehicle communication for joint perception and prediction. *European Conference on Computer Vision*, pages 605–621, 2020. 3
- [31] Wenjie Wang, Yehao Lu, Guangcong Zheng, Shuigen Zhan, Xiaoqing Ye, Zichang Tan, Jingdong Wang, Gaoang Wang, and Xi Li. Bevsprad: Spread voxel pooling for bird’s-eye-view representation in vision-based roadside 3d object detection. In *Proceedings of the IEEE/CVF Conference on Computer Vision and Pattern Recognition*, pages 14718–14727, 2024. 2
- [32] Hao Xiang, Zhaoliang Zheng, Xin Xia, Runsheng Xu, Letian Gao, Zewei Zhou, Xu Han, Xinkai Ji, Mingxi Li, Zonglin Meng, et al. V2x-real: a large-scale dataset for vehicle-to-everything cooperative perception. *arXiv preprint arXiv:2403.16034*, 2024. 2
- [33] Baowei Xu, Xinyu Zhang, Li Wang, Xiaomei Hu, Zhiwei Li, Shuyue Pan, Jun Li, and Yongqiang Deng. Rpf-net: A 4d radar pillar feature attention network for 3d object detection. In *IEEE International Intelligent Transportation Systems Conference (ITSC)*, pages 3061–3066, 2021. 6, 7, 13
- [34] Runsheng Xu, Yi Guo, Xu Han, Xia Xin, Xiang Hao, and Ma Jiaqi. Opencda: an open cooperative driving automation framework integrated with co-simulation. In *IEEE International Intelligent Transportation Systems Conference (ITSC)*, pages 1155–1162, 2021. 2
- [35] Runsheng Xu, Zhengzhong Tu, Xiang Hao, Wei Shao, Bolei Zhou, and Ma Jiaqi. Cobevt: Cooperative bird’s eye view semantic segmentation with sparse transformers. In *CONFERENCE ON ROBOT LEARNING*, pages 989–1000, 2022. 3, 7
- [36] Runsheng Xu, Hao Xiang, Zhengzhong Tu, Xin Xia, Ming-Hsuan Yang, and Jiaqi Ma. V2x-vit: Vehicle-to-everything cooperative perception with vision transformer. In *European Conference on Computer Vision*, pages 107–124. Springer, 2022. 2, 3, 7, 8
- [37] Runsheng Xu, Hao Xiang, Xin Xia, Xu Han, Jinlong Li, and Jiaqi Ma. Opv2v: An open benchmark dataset and fusion pipeline for perception with vehicle-to-vehicle communication. In *2022 International Conference on Robotics and Automation (ICRA)*, pages 2583–2589, 2022. 2, 3
- [38] Runsheng Xu, Xiang Hao, Xu Han, Xia Xin, Zonglin Meng, Chia Ju Chen, Camila Correa Jullian, and Ma Jiaqi. The opencda open-source ecosystem for cooperative driving automation research. *IEEE TRANSACTIONS ON INTELLIGENT VEHICLES*, 8(4):2698–2711, 2023. 2
- [39] Runsheng Xu, Xin Xia, Jinlong Li, Hanzhao Li, Shuo Zhang, Zhengzhong Tu, Zonglin Meng, Hao Xiang, Xiaoyu Dong, Rui Song, et al. V2v4real: A real-world large-scale dataset for vehicle-to-vehicle cooperative perception. In *Proceedings of the IEEE/CVF Conference on Computer Vision and Pattern Recognition*, pages 13712–13722, 2023. 2, 3, 7
- [40] Yan Yan, Yuxing Mao, and Bo Li. Second: Sparsely embedded convolutional detection. *Sensors*, 18(10):3337, 2018. 6, 7, 13
- [41] Lei Yang, Tao Tang, Jun Li, Peng Chen, Kun Yuan, Li Wang, Yi Huang, Xinyu Zhang, and Kaicheng Yu. Bevheight++: Toward robust visual centric 3d object detection. *arXiv preprint arXiv:2309.16179*, 2023. 2, 6, 7, 13
- [42] Lei Yang, Kaicheng Yu, Tao Tang, Jun Li, Kun Yuan, Li Wang, Xinyu Zhang, and Peng Chen. Bevheight: A robust framework for vision-based roadside 3d object detection. In *Proceedings of the IEEE/CVF Conference on Computer Vision and Pattern Recognition*, pages 21611–21620, 2023. 2, 6, 7, 13
- [43] Lei Yang, Xinyu Zhang, Jun Li, Li Wang, Minghan Zhu, Chuang Zhang, and Huaping Liu. Mix-teaching: A simple, unified and effective semi-supervised learning framework for monocular 3d object detection. *IEEE Transactions on Circuits and Systems for Video Technology*, 33(11):6832–6844, 2023. 2

- [44] Lei Yang, Xinyu Zhang, Jun Li, Li Wang, Chuang Zhang, Li Ju, Zhiwei Li, and Yang Shen. Sgv3d: Towards scenario generalization for vision-based roadside 3d object detection. *arXiv preprint arXiv:2401.16110*, 2024. 2
- [45] Lei Yang, Xinyu Zhang, Jiaxin Yu, Jun Li, Tong Zhao, Li Wang, Yi Huang, Chuang Zhang, Hong Wang, and Yiming Li. Monogae: Roadside monocular 3d object detection with ground-aware embeddings. *IEEE Transactions on Intelligent Transportation Systems*, 2024. 2
- [46] Xiaoqing Ye, Mao Shu, Hanyu Li, Yifeng Shi, Yingying Li, Guangjie Wang, Xiao Tan, and Errui Ding. Rope3d: The roadside perception dataset for autonomous driving and monocular 3d object detection task. In *Proceedings of the IEEE/CVF Conference on Computer Vision and Pattern Recognition*, pages 21341–21350, 2022. 6
- [47] Tianwei Yin, Xingyi Zhou, and Philipp Krahenbuhl. Center-based 3d object detection and tracking. In *Proceedings of the IEEE/CVF Conference on Computer Vision and Pattern Recognition*, pages 11784–11793, 2021. 6, 7, 13
- [48] Haibao Yu, Yizhen Luo, Mao Shu, Yiyi Huo, Zebang Yang, Yifeng Shi, Zhenglong Guo, Hanyu Li, Xing Hu, Jirui Yuan, et al. Dair-v2x: A large-scale dataset for vehicle-infrastructure cooperative 3d object detection. In *Proceedings of the IEEE/CVF Conference on Computer Vision and Pattern Recognition*, pages 21361–21370, 2022. 2, 3, 7
- [49] Haibao Yu, Wenxian Yang, Hongzhi Ruan, Zhenwei Yang, Yingjuan Tang, Xu Gao, Xin Hao, Yifeng Shi, Yifeng Pan, Ning Sun, et al. V2x-seq: A large-scale sequential dataset for vehicle-infrastructure cooperative perception and forecasting. In *Proceedings of the IEEE/CVF Conference on Computer Vision and Pattern Recognition*, pages 5486–5495, 2023. 2, 3
- [50] Haibao Yu, Yingjuan Tang, Enze Xie, Jilei Mao, Ping Luo, and Zaiqing Nie. Flow-based feature fusion for vehicle-infrastructure cooperative 3d object detection. *Advances in Neural Information Processing Systems*, 36, 2024. 3
- [51] Haibao Yu, Wenxian Yang, Jiaru Zhong, Zhenwei Yang, Siqi Fan, Ping Luo, and Zaiqing Nie. End-to-end autonomous driving through v2x cooperation. In *The 39th Annual AAAI Conference on Artificial Intelligence*, 2025. 3
- [52] Xinyu Zhang, Li Wang, Jian Chen, Cheng Fang, Lei Yang, Ziyang Song, Guangqi Yang, Yichen Wang, Xiaofei Zhang, Qingshan Yang, and Jun Li. Dual radar: A multi-modal dataset with dual 4d radar for autonomous driving. *arXiv preprint arXiv:2310.07602*, 2023. 2, 3
- [53] Tong Zhao, Yichen Xie, Mingyu Ding, Lei Yang, Masayoshi Tomizuka, and Yintao Wei. A road surface reconstruction dataset for autonomous driving. *Scientific data*, 11(1):459, 2024. 2
- [54] Tong Zhao, Lei Yang, Yichen Xie, Mingyu Ding, Masayoshi Tomizuka, and Yintao Wei. Roadbev: Road surface reconstruction in bird’s eye view. *IEEE Transactions on Intelligent Transportation Systems*, 25(11):19088–19099, 2024. 2
- [55] Walter Zimmer, Gerhard Arya Wardana, Suren Sritharan, Xingcheng Zhou, Rui Song, and Alois C Knoll. Tumor v2x cooperative perception dataset. In *Proceedings of the IEEE/CVF Conference on Computer Vision and Pattern Recognition*, pages 22668–22677, 2024. 3

# V2X-Radar: A Multi-modal Dataset with 4D Radar for Cooperative Perception

## Supplementary Material

### A. Appendix

This supplementary document is organized as follows:

- We offer further details on the time synchronization of sensors on vehicle and roadside platforms in Appendix B.
- We provide supplementary benchmark results, which include roadside 3D object detection on V2X-Radar-I sub-dataset and vehicle-side 3D object detection on V2X-Radar-V sub-dataset, both evaluated under heterogeneous splits in Appendix C.
- We provide visualizations of different data collection scenarios, including corner cases for single-vehicle autonomous driving and a variety of time-of-day and weather conditions in Appendix D.

### B. Synchronization Details

Time synchronization enables the simultaneous sampling of data from the same scene by various sensors on both the vehicle platform and roadside units. For a collaborative perception dataset, achieving precise time alignment is critical—not only among the diverse sensors within a single platform (be it the vehicle or the roadside unit) but also across sensors spanning both platforms.

The solution for time synchronization in our V2X-Radar is illustrated in Fig. 7. Typically, the vehicle platform and roadside unit align their sensors using a synchronization box that leverages the Precision Time Protocol (PTP). This synchronization box integrates Pulse Per Second (PPS) signals and Time of Day (ToD) data sourced from the GPS/IMU system. The process entails generating PTP timing signals to synchronize industrial computers, which subsequently facilitate hardware-triggered synchronization for LiDAR and 4D Radar. The PPS signals act as hardware triggers for camera data acquisition, utilizing rising edge pulses to ensure alignment between cameras, LiDAR, and 4D Radar within the same platform. To achieve time synchronization between the vehicle platform and the roadside unit, both systems receive identical GNSS signals from GPS satellites, ensuring precise clock alignment of the GPS/IMU systems across the two platforms.

### C. More Benchmark Results

We present benchmark results for single-agent 3D object detection, which include roadside 3D object detection on the V2X-Radar-I sub-dataset and single-vehicle 3D object detection on the V2X-Radar-V sub-dataset. All methods are evaluated using the heterogeneous split.

### C.1. Roadside 3D Object Detection

Tab. 6 presents a quantitative evaluation of multiple roadside 3D object detection models, leveraging our V2X-Radar-I sub-dataset under a heterogeneous split configuration. The results reveal that:

- LiDAR-based methods achieve the best performance, while 4D Radar and camera-based methods are less effective than LiDAR. Furthermore, the performance of 4D Radar and camera-based methods is comparable; 4D Radar excels at IoU=0.5, while camera-based methods perform better at the stricter IoU=0.7.
- Compared to the results in Tab.4, both camera-based and 4D Radar-based roadside methods under the heterogeneous split show a significant decline in performance, highlighting that scenario generalization presents a challenge for both methods.

### C.2. Single-vehicle 3D Object Detection

Tab. 7 presents comparative experiments of various single-vehicle 3D object detection models utilizing our V2X-Radar-V sub-dataset under a heterogeneous split. It is evident from the table that:

- LiDAR-based methods demonstrate the highest performance. 4D Radar-based methods outperform camera-based methods but do not match the effectiveness of LiDAR-based approaches, exhibiting slight deviations from the results in Tab. 6.
- In comparison to the findings presented in Tab. 5, both camera-based and 4D Radar single-vehicle approaches under the heterogeneous split exhibit markedly reduced performance. This underscores the substantial difficulties these methods face in achieving robust generalization across diverse scenarios.

### D. Data Collection Scenarios

Our data collection encompasses various weather conditions and times of day, focusing on challenging corner cases for single-vehicle autonomous driving. Fig. 8 presents a visual depiction of various challenging corner cases, such as occluded vehicles at a public intersection, partially hidden cyclists at a public T-junction, concealed pedestrians within a restricted park environment, and obscured cyclists at a campus intersection. Fig. 9 illustrates the scenarios employed for data acquisition, spanning diverse times of day and meteorological conditions. As highlighted in Fig. 9(a), the temporal segments include morning daytime, afternoon daytime, dusk, and nighttime. As shown in Figure 9(b),

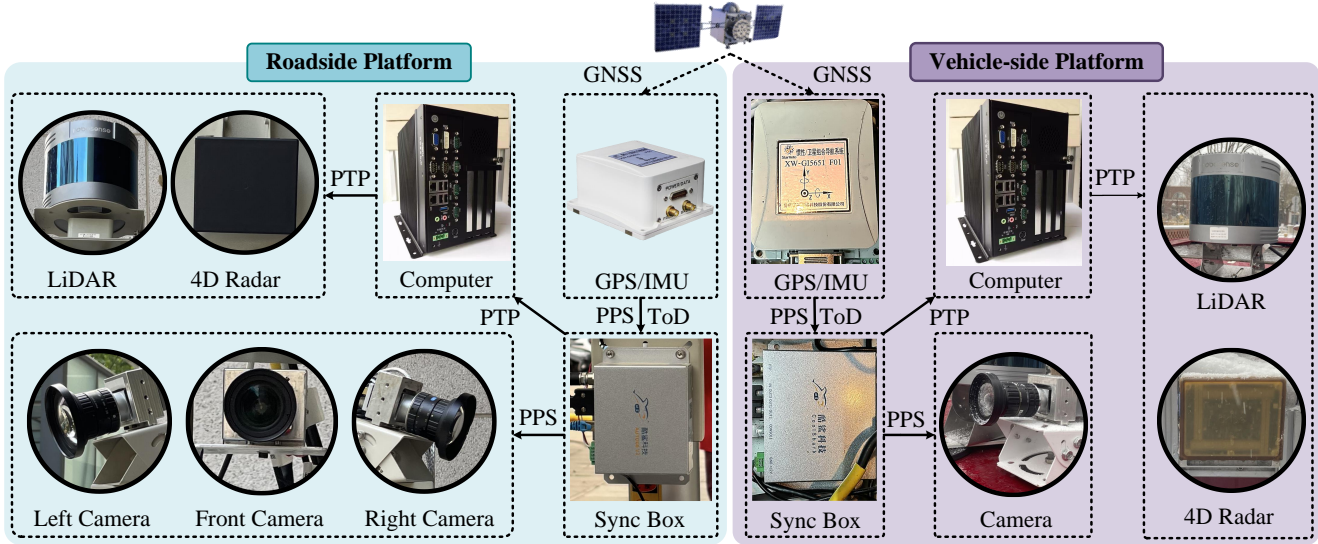


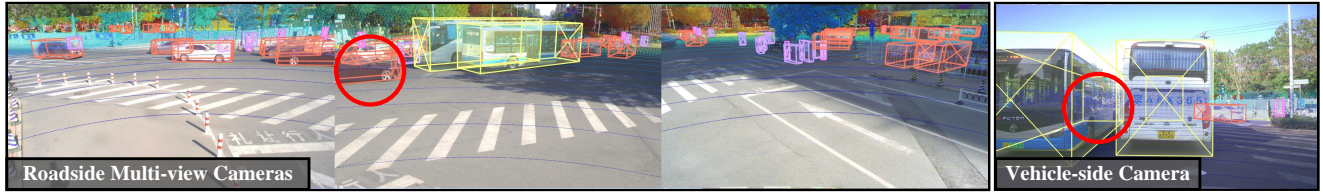
Figure 7. **The time synchronization solution for the connected vehicle-side platform and the intelligent roadside unit.** Both the vehicle platform and roadside unit are equipped with a computer, a time synchronization box, a GPS/IMU system, and various sensors, including LiDAR, 4D radar, and cameras. The GPS/IMU systems in both the vehicle platform and roadside unit receive the same GNSS signals from GPS satellites.

Table 6. **Roadside 3D object detection benchmarks on V2X-Radar-I under the heterogeneous split.** The vehicle category includes car, bus and truck. ‘M’ means modality, and L, C, and R denote LiDAR, Camera, and 4D Radar, respectively.

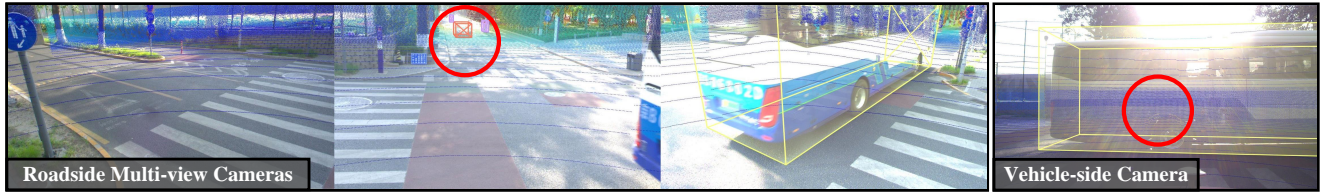
Method	M	Vehicle (IoU = 0.7 / 0.5)			Pedestrian (IoU = 0.5 / 0.25)			Cyclist (IoU = 0.5 / 0.25)		
		Easy	Moderate	Hard	Easy	Moderate	Hard	Easy	Moderate	Hard
Pointpillars [11]	L	66.19 / 86.11	61.28 / 78.82	61.28 / 78.82	33.32 / 49.80	27.79 / 41.28	27.79 / 41.28	64.87 / 74.11	56.55 / 64.95	56.55 / 64.95
SECOND [40]	L	68.93 / 86.82	62.11 / 79.48	62.11 / 79.48	39.76 / 56.78	32.83 / 47.03	32.83 / 47.03	69.73 / 77.73	60.79 / 68.29	60.79 / 68.29
CenterPoint [47]	L	70.87 / 87.62	65.62 / 80.22	65.63 / 80.22	57.66 / 71.58	47.29 / 59.34	47.29 / 59.34	73.08 / 78.15	65.46 / 70.27	65.46 / 70.27
PV-RCNN [21]	L	82.08 / 92.27	74.75 / 84.81	74.75 / 84.81	67.33 / 80.39	56.72 / 66.69	56.72 / 66.69	76.59 / 82.04	67.11 / 72.51	67.11 / 72.51
SMOKE [15]	C	3.04 / 16.87	2.99 / 16.64	2.99 / 16.63	0.05 / 0.09	0.04 / 0.07	0.04 / 0.07	1.12 / 8.25	1.07 / 7.47	1.07 / 7.39
BEVDepth [13]	C	12.24 / 23.06	11.45 / 21.76	10.72 / 21.58	0.08 / 2.11	0.06 / 0.86	0.06 / 0.86	1.75 / 12.92	1.56 / 10.24	1.55 / 10.13
BEVHeight [42]	C	12.94 / 24.41	11.61 / 23.55	11.40 / 23.35	1.01 / 3.11	0.08 / 1.29	0.08 / 1.24	3.31 / 18.14	2.01 / 12.24	2.01 / 12.22
BEVHeight++[41]	C	14.07 / 25.12	13.57 / 24.81	13.25 / 24.62	1.39 / 4.87	0.13 / 1.63	0.13 / 1.62	4.20 / 19.69	2.57 / 12.81	2.57 / 12.78
RDIOU [20]	R	4.31 / 25.74	3.85 / 24.24	3.85 / 24.24	1.55 / 8.64	1.16 / 6.96	1.16 / 6.96	1.94 / 10.91	1.55 / 9.65	1.55 / 9.65
RPFA-Net [33]	R	4.49 / 28.39	4.18 / 26.39	4.18 / 26.39	1.76 / 7.82	1.32 / 7.04	1.32 / 7.04	2.36 / 12.61	1.95 / 10.94	1.95 / 10.94

Table 7. **Single-vehicle 3D object detection benchmarks on V2X-Radar-V under the heterogeneous split.** The vehicle category includes car, bus and truck. ‘M’ means modality, and L, C, and R denote LiDAR, Camera, and 4D Radar, respectively.

Method	M	Vehicle (IoU = 0.7 / 0.5)			Pedestrian (IoU = 0.5 / 0.25)			Cyclist (IoU = 0.5 / 0.25)		
		Easy	Moderate	Hard	Easy	Moderate	Hard	Easy	Moderate	Hard
Pointpillars [11]	L	72.03 / 80.43	64.65 / 72.87	64.65 / 71.87	39.01 / 44.17	33.37 / 40.17	33.37 / 40.17	72.46 / 75.99	61.97 / 65.82	61.97 / 65.82
SECOND [40]	L	75.13 / 83.37	66.06 / 76.08	66.06 / 76.08	41.63 / 46.39	35.34 / 42.69	35.34 / 42.69	75.17 / 80.84	63.07 / 69.71	63.07 / 69.71
CenterPoint [47]	L	77.67 / 85.22	67.24 / 78.26	67.24 / 78.26	53.77 / 57.67	48.08 / 54.68	48.08 / 54.68	83.92 / 89.51	72.69 / 75.69	72.69 / 75.69
PV-RCNN [21]	L	83.34 / 87.91	77.37 / 81.24	77.37 / 81.24	62.33 / 63.18	56.87 / 59.87	56.87 / 59.87	86.68 / 91.54	76.73 / 78.05	76.73 / 78.05
SMOKE [15]	C	0.31 / 7.28	0.16 / 3.81	0.16 / 3.74	0.03 / 0.18	0.02 / 0.11	0.02 / 0.11	0.08 / 1.89	0.07 / 1.25	0.07 / 1.25
BEVDepth [13]	C	1.23 / 9.67	0.58 / 5.57	0.58 / 5.41	0.06 / 1.02	0.04 / 0.71	0.04 / 0.71	1.01 / 3.74	0.05 / 1.91	0.05 / 1.91
BEVHeight [42]	C	1.12 / 9.79	0.56 / 4.89	0.53 / 4.43	0.05 / 0.93	0.04 / 0.69	0.04 / 0.69	0.09 / 3.34	0.05 / 1.89	0.05 / 1.89
BEVHeight++[41]	C	1.79 / 14.26	0.62 / 7.61	0.58 / 6.87	0.07 / 1.83	0.06 / 1.16	0.06 / 1.16	0.13 / 3.91	0.07 / 2.31	0.07 / 2.28
RDIOU [20]	R	3.77 / 34.43	3.48 / 19.03	3.37 / 17.74	0.04 / 0.75	0.02 / 0.62	0.02 / 0.62	0.88 / 8.94	0.29 / 4.15	0.29 / 4.15
RPFA-Net [33]	R	4.23 / 35.49	3.81 / 19.44	3.62 / 18.63	0.04 / 0.95	0.03 / 0.81	0.03 / 0.81	1.24 / 11.01	0.57 / 5.49	0.57 / 5.49



(a) The car is occluded at a public intersection.



(b) The car is occluded at a campus intersection



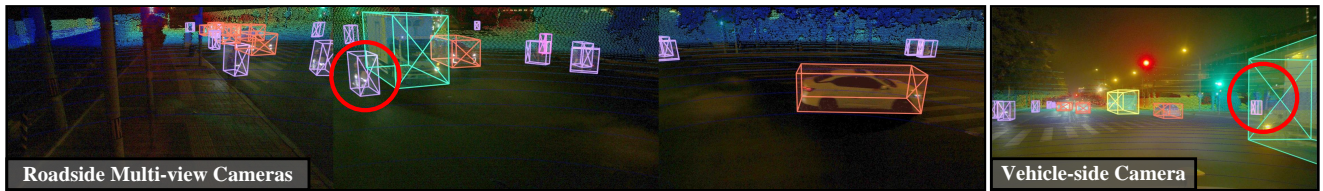
(c) The car is occluded at a campus T-junction



(d) The pedestrian is occluded at a closed park



(e) The cyclist is occluded at a campus T-junction.



(f) The cyclist is occluded at a public T-junction



(g) The cyclist is obscured at a campus intersection

Figure 8. **Diverse corner cases for single-vehicle autonomous driving.** Each case is depicted by roadside multi-view images on the left and the vehicle-side image on the right. We use a red circle to mark the occluded objects.



(a) Different periods of the day



(b) Various weather conditions

Figure 9. **Data collection across different periods and various weather conditions.** a) Different times of day, including daytime, dusk, and nighttime. b) Various weather conditions like sunshine, rain, fog, and snow.

the weather conditions range from clear sunny skies to fog, rain, and snow.